Numerical study on the gas heating mechanism in pulse-modulated radio-frequency glow discharge*

Qi Wang(王奇), Xiao-Li Yu(于晓丽), and De-Zhen Wang(王德真)†

School of Physics and Optoelectronic Engineering, Key Laboratory of Materials Modification by Laser, Ion and Electron Beams, Chinese Ministry of Education, Dalian University of Technology, Dalian 116023, *China*

(Received 24 October 2016; revised manuscript received 8 December 2016; published online 18 January 2017)

The gas heating mechanism in the pulse-modulated radio-frequency (rf) discharge at atmospheric pressure was investigated with a one-dimensional two-temperature fluid model. Firstly, the spatiotemporal profiles of the gas temperature (T_g) in both consistent rf discharge and pulse-modulated rf discharge were compared. The results indicated that T_g decreases considerably with the pulse-modulated power, and the elastic collision mechanism plays a more important role in the gas heating change. Secondly, the influences of the duty cycle on the discharge parameters, especially on the T_g, were studied. It was found that T_g decreases almost linearly with the reduction of the duty cycle, and there exists one ideal value of the duty cycle, by which both the T_g can be adjusted and the glow mode can be sustained. Thirdly, the discharge mode changing from α to γ mode in the pulse-modulated rf discharge was investigated, the spatial distributions of T_g in the two modes show different features and the ion Joule heating is more important during the mode transition.

Keywords: gas heating, pulse-modulated rf discharge, atmospheric pressure glow discharge

PACS: 52.20.–j, 52.25.–b, 52.40.Kh **DOI:** 10.1088/1674-1056/26/3/035201

1. Introduction

Recently, there has been increased interest in non-thermal atmospheric pressure plasmas because of the capability of producing reactive species without expensive vacuum systems.[1–4] Among all kinds of power sources, the ratio-frequency (rf) power is almost the favorite one due to its advantage of lower breakdown voltage, higher density of reactive species, and easier generation of uniform glow plasmas.[5,6] However, its applications were restricted due to the relatively higher gas heating power compared to low frequency discharges.[7]

Pulse-modulated rf plasmas at high pressures have drawn intensive attention because they possess not only the trait of high density of reactive species of rf voltage power sources but also good control of plasma parameters.[8] Correspondingly, the discharge characteristics varying with modulated pulse frequencies and pulse widths[9] were studied experimentally and numerically in helium respectively. Some other works were also carried out, such as self-organized patterns[10] and the metastable particles in this discharge apparatus.[11] Recently, several groups claimed experimentally that pulse-modulation of the rf power could significantly change the gas temperature (T_g).[12–14]

Theoretical models simulating T_g for a self-consistent, non-equilibrium plasma discharge have been developed over the last 50 years. Pytte and Winsor[15] gave a simple two-temperature theoretical model for atmospheric helium arc plasma in a cylindrical duct. In the analysis, the radiation was ignored and plasma compositions were obtained from the Saha equation evaluated at the electron temperature (T_e). In 1991, a non-equilibrium model was developed to predict the two-dimensional flow, electron and heavy particle temperatures, and number density distributions in cascaded arcs of monatomic gases.[16] Recently, Sakiyama used a one-dimensional non-equilibrium model to simulate the continuous wave rf atmosphere pressure glow discharge (APGD). He compared the results of considering T_g with and without the energy conservation equation for heavy particles, and found that there was little difference between them.[17] The T_g at the atmospheric pressure conditions was measured experimentally in 2008.[18] In 2012, a two-temperature non-equilibrium chemical model of the commercial code CFD-ACE+[19] was used to describe the tungsten inert gas arcs at atmospheric pressure. The energy conservation equations of electrons and heavy particles were treated separately, including the reaction heat terms and particle density gradients in this model, by which the heat transfer was described self-consistently. The system descriptions for the mechanism of gas heating can also be found elsewhere,[20,21] while the T_g in the discharge driven by pulse-modulated rf power at the atmospheric pressure has not been investigated quantitatively before.

In this paper, the T_g characteristics in the pulse-modulated rf glow discharge at atmospheric pressure conditions are investigated and the gas heating mechanisms are revealed with a one-dimensional two-temperature fluid non-equilibrium model. The spatiotemporal graphs of T_g in consistent rf dis-

*Project supported by the National Natural Science Foundation of China (Granted Nos. 11405022 and 11475040) and Dalian High Level Talent Innovation Support Plan, China (Grant No. 2015R050).

†Corresponding author. E-mail: wangdez@dlut.edu.cn

© 2017 Chinese Physical Society and IOP Publishing Ltd

charge and pulse-modulated rf discharge are compared, then the T_e feature is also described. Additionally, the influences of the duty cycle on T_g are studied. Finally, the discharge mode changing from α to γ mode in the pulse-modulated rf discharge is investigated and the gas heating mechanisms are analyzed.

2. Numerical model

The discharge is generated between two plane electrodes at atmospheric pressure. The pulse modulated rf voltage is applied to the upper electrode while the lower electrode is grounded. Helium is taken as the working gas, and five species are considered in the model: electrons (e), atomic ions (He^+), molecular ions (He_2^+), atomic metastable (He^*), and molecular metastable (He_2^*). The particle densities are governed by the continuity equations

$$\frac{\partial n_{e,i,m}}{\partial t} + \frac{\partial j_{e,i,m}}{\partial x} = S_{e,i,m}, \tag{1}$$

where n is the particle's number density, S is the sum of source and loss terms of specific species resulting from series of reactions which are summarized in Table 1, and the subscripts e, i, and m represent electron, ion, and metastable, respectively.

Table 1. Reactions considered in the present work. The rate coefficient is in units of $cm^3 \cdot s^{-1}$ for two-body reactions and in units of $cm^6 \cdot s^{-1}$ for three-body reactions.

Reaction	No.	Reaction	Rate coefficient	Ref.
Excitation and ionization	R1	$e + He \rightarrow He^+ + 2e$	α	[22]
	R2	$e + He \rightarrow He^* + e$	$4.2\times10^{-9} T_e^{0.31} e_e^{-19.8/T}$	[23]
	R3	$e + He^* \rightarrow He^+ + 2e$	$1.28\times10^{-7} T_e^{0.6} e_e^{-4.78/T}$	[23]
Recombination and de-excitation	R4	$He_2^+ + e \rightarrow He^* + He$	5.0×10^{-9}	[24]
	R5	$He_2^+ + e \rightarrow 2He^*$	4.0×10^{-9}	[24]
	R6	$He^+ + e \rightarrow He$	$8.1\times10^{-20}(n_e/(1+0.079p))(T_e/T_g)^{-4.4}$	[25]
	R7	$He^* + e \rightarrow He + e$	2.9×10^{-9}	[26]
Metastable and ion conversion	R8	$He^+ + 2He \rightarrow He_2^+ + He$	2.0×10^{-31}	[23]
	R9	$He^* + 2He \rightarrow He_2^* + He$	1.5×10^{-34}	[26]
Associative ionization	R10	$He^* + He^* \rightarrow e + He^+ + He$	8.7×10^{-10}	[27]
	R11	$He^* + He^* \rightarrow e + He_2^+$	2.03×10^{-9}	[27]
	R12	$He_2^* + He_2^* \rightarrow He_2^+ + 2He + e$	1.28×10^{-10}	[25]
	R13	$He_2^* + He_2^* \rightarrow He^+ + 3He + e$	2.25×10^{-11}	[25]
	R14	$He^* + He_2^* \rightarrow He_2^+ + He + e$	1.28×10^{-10}	[25]
	R15	$He^* + He_2^* \rightarrow He^+ + 2He + e$	2.25×10^{-11}	[25]

The particle flow density j is computed via the diffusion-drift approximation

$$j_{e,i} = \mp\mu_{e,i} n_{e,i} E - D_{e,i}\frac{\partial n_{e,i}}{\partial x}, \tag{2}$$

$$j_m = -D_m \frac{\partial n_m}{\partial x}, \tag{3}$$

where μ and D are the mobility and diffusion coefficients, which have been listed distinctly in Table 1 in Ref. [28] as a function of gas density and gas temperature. The mobility of charged species is assumed to be constant, and the diffusivity is assumed to follow Einstein's relation. The electrical field E is obtained by solving the current conservation equation instead of solving Poisson's equation

$$\varepsilon\frac{\partial E(x,t)}{\partial t} + j_c(x,t) = j_0(t), \tag{4}$$

where j_c is the conductive current density calculated by $j_c = q(j_i - j_e)$, with q being the unit charge of 1.6×10^{-19} C, j_0 is the total current density, and ε is the permittivity, taking either ε_0 in the discharge gap or $\varepsilon_0\varepsilon_b$ in the dielectric barrier layer. The energy conservation equation for the electrons reads

$$\begin{aligned}&\frac{\partial}{\partial t}\left(\frac{3}{2}n_e k T_e\right) + \frac{\partial}{\partial x}\left(\frac{5}{2}kT_e j_e - \frac{3}{2}kD_e n_e\frac{\partial T_e}{\partial x}\right)\\ &+ e j_e E + \frac{3}{2}k(T_e - T_g)n_e\left(\frac{2m_e}{m_g}\right)\bar{\nu}_{eg}\\ &+ \sum_l \Delta E_l^e K_l = 0,\end{aligned} \tag{5}$$

where k is Boltzmann's constant, T_e is the electron temperature, m_e and m_g are the masses of electron and dominant background gas species, respectively, $\bar{\nu}_{eg}$ is the electron momentum transfer collision frequency with the background gas, ΔE_l^e is the energy lost per electron in an inelastic collision, and K_l is the rate-of-progress of reaction l. The second to the fifth terms on the left-hand side of Eq. (5) are the electron convection and conduction term, the electron Joule heating term, the rate of electron energy loss due to elastic collisions with heavy particles, and the energy exchange term between the electrons and the heavy species through inelastic collision, respectively.[29]

The T_g is solved by the equation

$$\begin{aligned}&\frac{\partial}{\partial t}\left(\frac{3}{2}n_g k T_g\right) + \frac{\partial}{\partial x}\left(\frac{5}{2}kT_g j_g\right) - \frac{\partial}{\partial x}\left(\lambda_{eff}\frac{\partial kT_g}{\partial x}\right)\\ &= \frac{3}{2}k(T_e - T_g)n_e\left(\frac{2m_e}{m_g}\right)\bar{\nu}_{eg}\\ &+ \sum_j \Delta E_j^g K_j + \sum_i e j_i E,\end{aligned} \tag{6}$$

where n_g is the heavy-particle number density (the sum of ions and neutral atoms), λ_{eff} is the thermal conductivity of the gas mixture, and ΔE_j^g is the bond or ionization energy of inelastic collision with heavy particles. The third term at the left-hand side of Eq. (5) represents the thermal flow of the gas. The three terms at the right-hand side of the equation are the contributions to the gas heating due to elastic collisions with electrons, the energy loss due to inelastic collision with heavy particles, and the effective ion Joule heating, respectively.[30,31] The flow chart for coupling calculation of the equations is given in Fig. 1, and the equations above are solved numerically with explicit S–G scheme.[32]

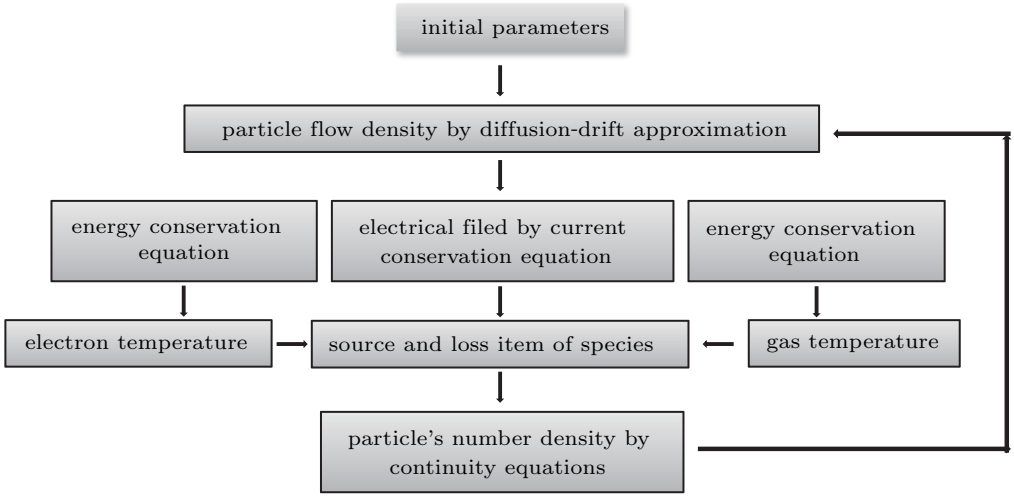


Fig. 1. Flow chart for coupling calculation of the equations.

3. Results and discussion

The simulation parameters are chosen as follows: the discharge gap is fixed at 2 mm, and the relative permittivity constant ε_b is set to 7.5. The gas pressure is 760 Torr, and the initial value of T_g is set to 300 K. The continuity boundary conditions are applied at the electrodes for the gas temperature. The secondary electron emission coefficient is assumed to be 0.01. The frequency of the rf power source is 13.56 MHz while the external voltage amplitude varies from 500 V to 600 V. The repetitive frequency of the pulse varies from 12.5 kHz to 100 kHz, and its width is set between 1 μs and 80 μs. The initial densities of electrons and atomic ions are both set to 1.0×10^7 cm^{-3}, and the densities of the other charged particles and the metastable species are 1.0×10^2 cm^{-3} in the whole discharge space. All the results presented in this paper are calculated after the discharge reaches fully periodically steady state.

3.1. Gas temperature of continuous wave rf discharge

The amplitude and frequency of the rf voltage applied in this part are fixed at 570 V and 13.56 MHz, respectively. The contour maps of T_g and T_e during one rf period are shown in Fig. 2. As shown in Fig. 2(a), the maximum of T_g in the middle region is 438.8 K and the value near the electrode is 432.2 K, which is consistent with the magnitude observed in the experiment.[18] It can be seen from Fig. 2(b) that the maximum of T_e (3.51 eV) appears in the sheath region near the electrode surface where a strong electric field exists. The reason for the reduction of T_e in the center of the discharge gap is that the majority of the gas ionization events take place there.

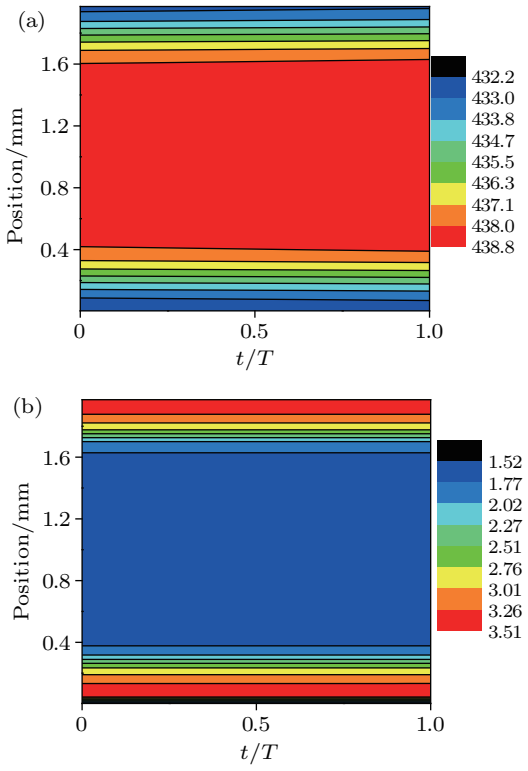


Fig. 2. (color online) (a) Spatial distributions of T_g (in units of K) and (b) T_e (in units of eV) during one rf cycle.

3.2. Gas temperature of pulse-modulated rf discharge

In order to assess the gas heating controlled by the modulated pulse source, we simulate the T_g with the same amplitude and frequency of the rf power as those (570 V, 13.56 MHz) in Subsection 3.1. The frequency of the pulse voltage is 12.5 kHz; the duty cycle of the power-on period is 30%, i.e., the width of one power-on time is set to 24 μs. After the discharge reaches its steady state, the waveforms of the driven voltage and discharge current density during about 1.5 pulse period are shown in Fig. 3. It can be seen from the figure that after the rf power is turned on, the discharge current density rises from almost zero to 65.9 mA/cm^2, while the discharge current density drops gradually to zero after the pulse is switched off.

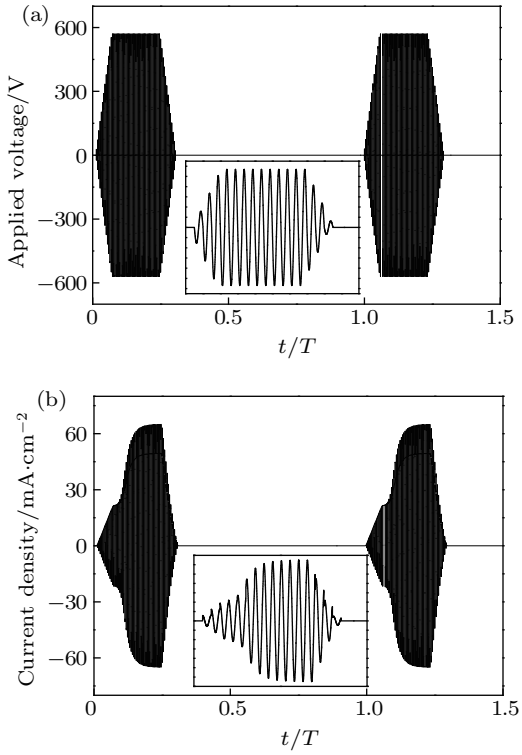


Fig. 3. Waveforms of (a) applied voltage and (b) discharge current density when driven by the pulse-modulated rf power.

The spatiotemporal distribution of T_g in pulse-modulated rf discharge during one pulse cycle is given in Fig. 4(a). It can be seen that, with 30% duty cycle, the maximal of T_g is 328.4 K, which is 110.4 K lower than that in the corresponding continuous wave discharge shown in Fig. 2(a). It means that T_g during the discharge could be significantly lowered by the pulse-modulation rf power; the reason is further explained later in Fig. 5. The spatiotemporal distribution of T_e in this case is given in Fig. 4(b). The peak value of T_e is 3.50 eV, which is nearly equal to the value of the consistent rf discharge shown in Fig. 2(b). We must note from the figures that T_e reaches its maximum after the power is turned on and drops abruptly after the power is off, which differs with the characteristics of T_g. It can be explained by the fact that the electrons gain and lose energy easily and quickly due to the relatively small mass compared to the ions.

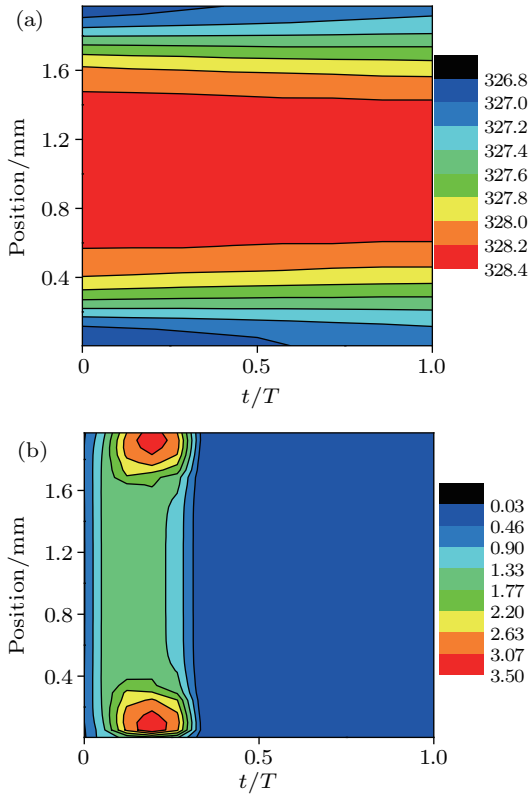


Fig. 4. (color online) Spatiotemporal distributions of (a) T_g(in units of K) and (b) T_e (in units of eV) for pulse-modulated rf discharge (30% duty cycle) during one pulse cycle.

Figure 5(a) shows the time averaged contributions of three gas heating mechanisms for the consistent rf discharge, i.e., the ion Joule heating, heating due to elastic collisions, and heating due to heavy particle reactions. It can be seen that the elastic collision (33.44 W/cm^3) is dominant in the central region (light cyan background) of the discharge; the ion Joule heating (23.28 W/cm^3) has a peak value in the sheath region (light gray background) near the electrode; while the heating due to the heavy particle reactions (23.33 W/cm^3) plays the most important role in the transition region between the sheath and the central regions. Figure 5(b) shows the same three mechanisms of T_g for the rf discharge with 30% duty cycle. We can see that the three components have similar spatial structures as those in the consistent rf discharge, while their magnitudes drop obviously. Being modulated by the pulse source, the maximum of heating due to elastic collisions in the central region is 4.94 W/cm^3. The peak value of ion Joule heating in the sheath region is 2.48 W/cm^3. The heating power due to heavy particles in the transition region reaches 3.55 W/cm^3. That is to say, the peak values of the heating due to elastic collisions, ion Joule heating, and heavy particle collisions decrease about 28.50 W/cm^3, 20.80 W/cm^3, and 19.78 W/cm^3, and drop to 14.8%, 10.7%, and 15.2%, respectively. It can be concluded that modulated by the pulse

power, each of the components contributing to the gas heating changes considerably, while the elastic collision plays a more important role on the gas temperature adjustment.

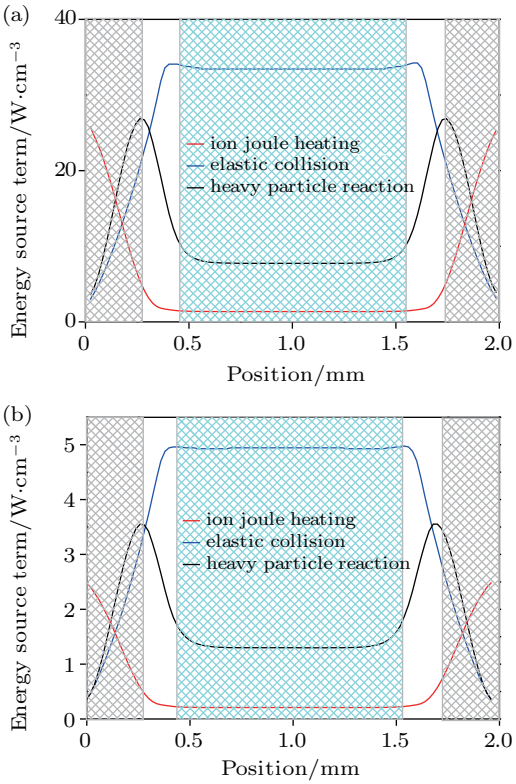


Fig. 5. (color online) Spatial distributions of the time averaged energy source terms for (a) consistent rf discharge and (b) pulse-modulated rf discharge with 12.5 kHz pulse frequency, 30% duty cycle.

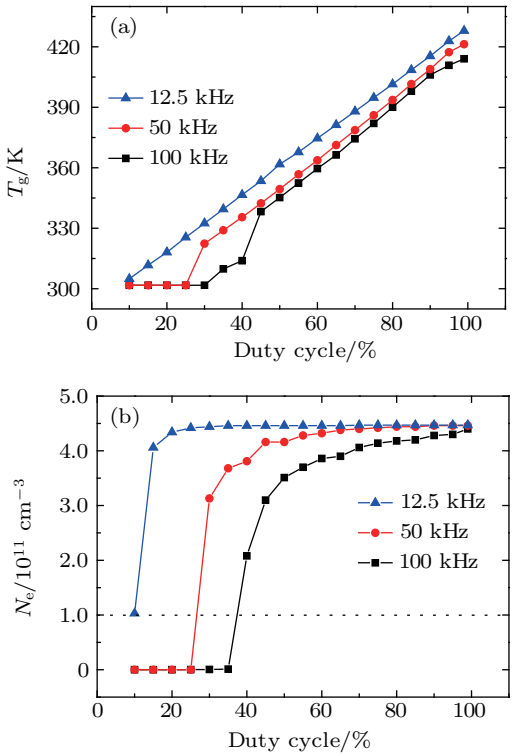


Fig. 6. (color online) The peak value of (a) T_g and (b) electron density varied with duty cycle for different pulse frequencies.

Next, we keep the frequency and amplitude of the rf voltage fixed and change the pulse frequency. The peak values of T_g and electron density (n_e) for three pulse frequencies (12.5 kHz, 50 kHz, 100 kHz) are shown in Fig. 6. As for the $f = 12.5$ kHz case (triangle symbols), $T_g = 420.0$ K when the duty cycle is 100%, then it decreases almost linearly with the reduction of the duty cycle, $T_g = 304.9$ K when the duty cycle is 10%. The gas temperature decreases about 120 K, which is commonly beneficial to the material in the industrial applications. It must be noted in addition that n_e would decrease below 1.0×10^{11} cm^{-3} if the duty cycle of the pulse source is adjusted lower than a specific duty cycle (10.2%), which means that the discharge may be changed from the glow mode to the Townsend mode. There is one ideal value of the duty cycle by which both T_g can be adjusted and the glow mode can be achieved. It can also be seen that the ideal duty cycles for the cases of 50 kHz and 100 kHz are 26.5% and 37.2%, respectively.

3.3. Gas temperatures of different modes in the pulse-modulated rf discharge

In order to investigate the T_g influenced by the external voltage, in this part, we keep all the parameters the same as those in Subsection 3.2 except the rf voltage amplitude. The parameters are as follows: the amplitude of the rf voltage varies from 510 V to 600 V while its frequency is fixed at 13.56 MHz. The frequency of the pulse voltage is 12.5 kHz, and the duty cycle of the power-on period is 50%, i.e., the width of the power-on is set to 40 μs. Figure 7(a) shows the discharge current density changes with the external voltage amplitude. The current density increases almost linearly with the rise of the voltage, while the value increases abruptly when the voltage amplitude exceeds 585 V, which is the same as the phenomenon of α–γ mode transition.[17] In the first mode, the α mode, the discharge current density is relatively low and the bulk plasma electrons obtain energy due to the sheath expansion. In the second mode, the γ mode, the discharge current density is relatively high, the secondary electrons emitted by the cathode under ion bombardment in the sheath region play an important role in sustaining the discharge.

Figure 7(b) describes the peak value of T_g increasing with the current density. It is obvious that the higher current leads to higher gas temperature under the same input voltage. Lower temperature can be obtained in the pulse-modulated rf glow discharge than that in the rf plasma discharge. With the same current density (for example 90 mA/cm^2 in the figure), the peak value of T_g in the pulse-modulated rf glow discharge (line with round symbols) is 390 K and the value in the consistent rf glow discharge (line with square symbols) is 608 K. Modulated by the pulse source with 12.5 kHz frequency and 50% duty cycle, the T_g is lowered by 218 K. This phenomenon has been observed in the experiment before.[2]

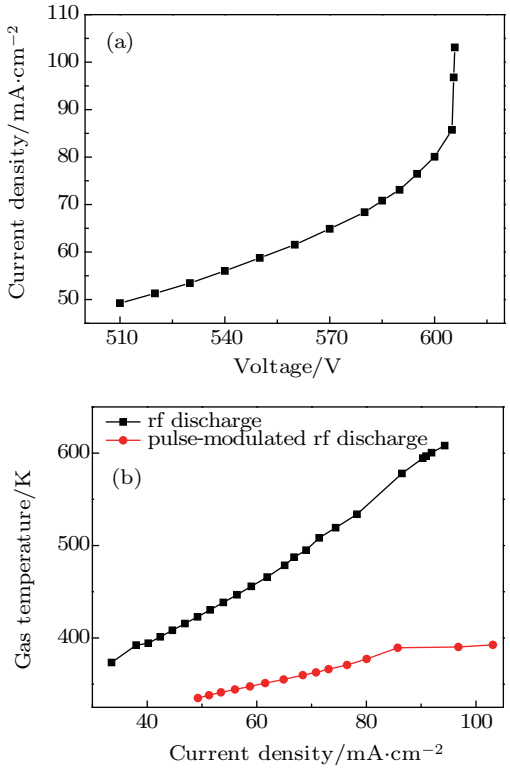


Fig. 7. (color online) (a) Discharge current varied with rf voltage amplitude; and (b) the peak value of T_g varied with current for both the rf discharge (square symbols) and the pulse modulated rf discharge.

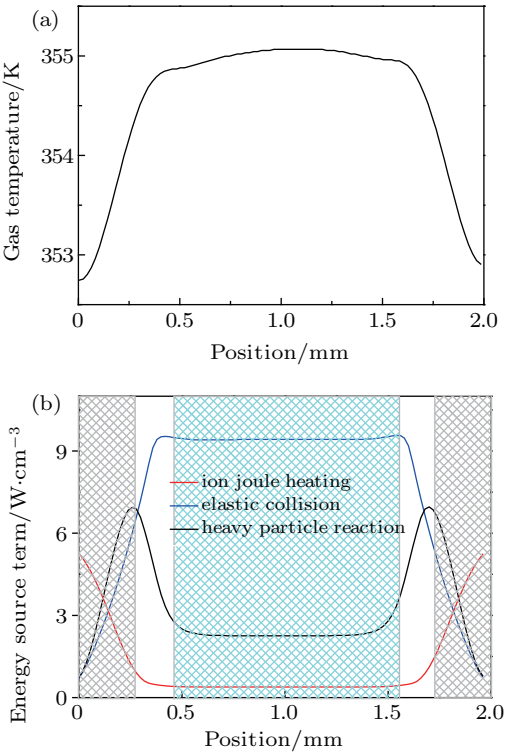


Fig. 8. (color online) Spatial distributions of (a) T_g and (b) energy source terms when $V_{rf} = 570$ V.

Figures 8(a) and 9(a) show the spatial distribution of T_g when the applied voltage amplitude is set to 570 V and 585 V, respectively. When V_{rf}= 570 V, one peak of T_g locates at the middle of the discharge gap; when $V_{rf} = 585$ V, two peaks of T_g appear near the electrodes. Moreover, the latter one (362 K) is higher than the former one (355 K).

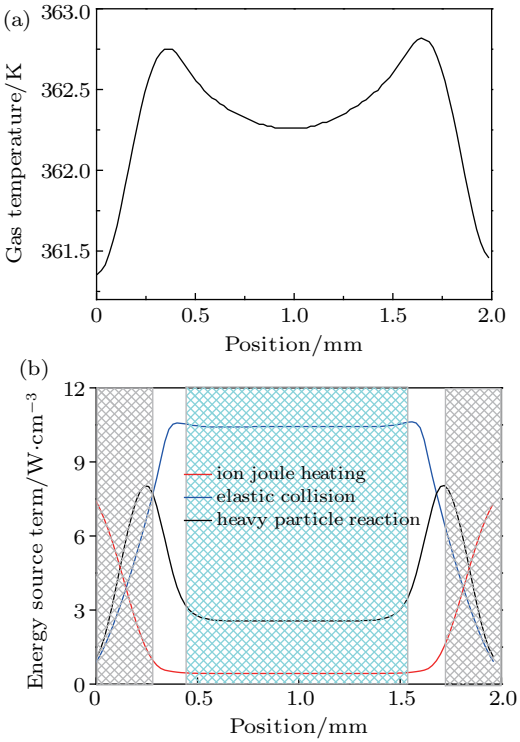


Fig. 9. (color online) Spatial distributions of (a) T_g and (b) energy source terms when $V_{rf} = 585$ V.

In order to investigate the mechanism of the transition from α to γ mode, we describe the contributions of the three mechanisms to the gas heating when the rf voltage amplitude is set to 570 V and 585 V in Figs. 8(b) and 9(b), respectively. It can be seen in the former case that the elastic collision (9.42 W/cm^3) is dominant in the central region of the discharge. The ion Joule heating (5.28 W/cm^3) has the peak value in the sheath region, while the heating due to the heavy particle reactions (6.94 W/cm^3) plays the most important role in the transition region between the sheath and the central regions. In the latter case, the maximum of heating due to elastic collisions in the central region is 10.43 W/cm^3, the ion Joule heating in the sheath region is 7.42 W/cm^3, and the heating due to heavy particles in the transition region is 8.00 W/cm^3. That is to say, the peak values of the heating due to elastic collisions, ion Joule heating, and heavy particle collisions increase about 1.01 W/cm^3, 2.14 W/cm^3, and 1.06 W/cm^3 by quantity, and 10.7%, 40.5%, and 15.3% by proportion, respectively. It can be concluded that for the transition from α to γ mode in pulse modulated rf discharge, each of the three contributions to the gas heating increases, while the ion Joule heating is more important during the mode transition.

4. Conclusion

The gas heating mechanisms in the pulse-modulated rf glow discharge have been investigated using a one-

dimensional two-temperature fluid model in this paper. It is found that T_g in the discharge can be controlled effectively by the pulse-modulated rf power, and the internal mechanisms are given. In the consistent rf discharge case, T_e drops abruptly while T_g would sustain for a longer time after the power is switched off due to the relatively small mass compared to the ions. Moreover, the influences of the duty cycle on the discharge parameters have been studied. It is revealed that T_g decreases almost linearly with the reduction of the duty cycle, and there is one ideal value of the duty cycle by which both the lower gas temperature and the glow mode can be achieved. In the further investigation, we have also found that the discharge mode changes from α to γ mode in the pulse-modulated rf discharge when the external voltage amplitude is increased. The spatial distributions of T_g for the two modes have different features and the ion Joule heating plays the most important role in the mode transition.

Acknowledgement

Qi Wang would like to thank Prof. Z. F. Ding for the useful discussion and the revision of the manuscript.

References

[1] Liu F C, He Y F and Wang X F 2014 *Chin. Phys. B* **23** 075209
[2] Sun J Z, Wang Q, Wang Y H, Zhang J H and Wang D Z 2008 *Chin. Phys. Lett.* **25** 4054
[3] He X, Dang W H and Jia H H 2014 *Chin. Phys. Lett.* **31** 95204
[4] Xu S J, Yao J and Bai M D 2012 *Acta Phys. Sin.* **61** 195202 (in Chinese)
[5] Yu Q, Deng Y F, Liu Y and Han X W 2008 *Chin. Phys. Lett.* **25** 2569
[6] Liu X M, Song Y H and Wang Y N 2011 *Chin. Phys. B* **20** 065205
[7] Kim D B, Jung H, Gweon B, Moon S Y, Rhee J K and Choe W 2011 *Phys. Plasmas* **18** 043503
[8] Shi J J, Zhang J, Qiu G, Walsh J L and Kong M G 2008 *Appl. Phys. Lett.* **93** 041502
[9] Sun J Z, Wang Q, Ding Z F, Li X C and Wang D Z 2011 *Phys. Plasmas* **18** 123502
[10] Wang Q, Sun J Z and Wang D Z 2012 *IEEE Trans. Plasma Sci. Tech.* **40** 35
[11] Wang Q, Sun J Z, Nozaki T, Ding Z F, Ding H B, Wang Z H and Wang D Z 2014 *Phys. Plasmas* **21** 083503
[12] Hu J T, Liu X Y, Liu J H and Xiong Z L 2012 *Phys. Plasmas* **19** 063505
[13] Ring Z, Mantei T D and Jackson H E 1995 *Appl. Phys. Lett.* **66** 3380
[14] Ishigaki T, Fan X and Sakuta T 1997 *Appl. Phys. Lett.* **71** 3787
[15] Pytte A and Winsor N K 1966 *Proc of 7th Int. Conf. Phenomena in Ionized Gases* **1** 709
[16] Beulens J J, Milojevic D and Schram D C 1991 *Physics of Fluids B: Plasma Physics* **3** 2548
[17] Sakiyama Y and Graves D B 2007 *J. Appl. Phys.* **7** 101
[18] Staack D, Farouk B, Gutsol A and Fridman A 2008 *Plasma Sources Sci. Technol.* **17** 025013
[19] Baeva M, Kozakov R and Gorchakov S 2012 *Plasma Sources Sci. Technol.* **13** 21
[20] Farouk T, Farouk B, Staack D, Gutsol A and Fridman A 2008 *Plasma Sources Sci. Technol.* **17** 035015
[21] Fridman A and Kennedy L A 2004 *Plasma Phys. Eng.* **22** 2011
[22] Ward A L 1962 *J. Appl. Phys.* **33** 2789
[23] Shon J W and Kushner M J 1994 *J. Appl. Phys.* **75** 1883
[24] Pouvesle J M, Bouchoule A and Stevefelt J J 1982 *Chem. Phys.* **77** 817
[25] Deloche R, Monchicourt P and Cheret M 1976 *Phys. Rev. A* **13** 1140
[26] Emmert F, Angermann H H, Dux R and Langhoff H 1988 *J. Phys. D: Appl. Phys.* **21** 667
[27] Stevefelt J, Pouvesle J M and Bouchoule A J 1982 *Chem. Phys.* **76** 4006
[28] Wang Q, Economou D J and Donnelly V M 2006 *J. Appl. Phys.* **100** 023301
[29] Shang W L, Wang D Z and Kong M G 2007 *Chin. Phys.* **16** 0485
[30] Chen D M and Pfender E 1981 *IEEE Trans. Plasma Sci.* **4** 0265
[31] Deconinck T and Raja L L 2009 *Plasma Process. Polym.* **6** 335
[32] Scharfetter D L and Gummel H K 1969 *IEEE Trans. Electron Devices* **16** 64